

Strategic Preys Make Acute Predators: Enhancing Camouflaged Object Detectors by Generating Camouflaged Objects

Chunming He¹, Kai Li^{2*}, Yachao Zhang¹, Yulun Zhang³,
Zhenhua Guo⁴, Xiu Li^{1*}, Martin Danelljan³, Fisher Yu³

¹Shenzhen International Graduate School, Tsinghua University,

²NEC Laboratories America, ³ETH Zürich, ⁴Tianyi Traffic Technology

Abstract

Camouflaged object detection (COD) is the challenging task of identifying camouflaged objects visually blended into surroundings. Albeit achieving remarkable success, existing COD detectors still struggle to obtain precise results in some challenging cases. To handle this problem, we draw inspiration from the prey-vs-predator game that leads preys to develop better camouflage and predators to acquire more acute vision systems and develop algorithms from both the prey side and the predator side. On the prey side, we propose an adversarial training framework, *Camouflageator*, which introduces an auxiliary generator to generate more camouflaged objects that are harder for a COD method to detect. *Camouflageator* trains the generator and detector in an adversarial way such that the enhanced auxiliary generator helps produce a stronger detector. On the predator side, we introduce a novel COD method, called *Internal Coherence and Edge Guidance (ICEG)*, which introduces a camouflaged feature coherence module to excavate the internal coherence of camouflaged objects, striving to obtain more complete segmentation results. Additionally, *ICEG* proposes a novel edge-guided separated calibration module to remove false predictions to avoid obtaining ambiguous boundaries. Extensive experiments show that *ICEG* outperforms existing COD detectors and *Camouflageator* is flexible to improve various COD detectors, including *ICEG*, which brings state-of-the-art COD performance.

1. Introduction

The never-ending prey-vs-predator game drives preys to develop various escaping strategies. One of the most effective and ubiquitous strategies is camouflage. Preys use camouflage to blend into the surrounding environment, striving to escape hunting from predators. For survival, predators,

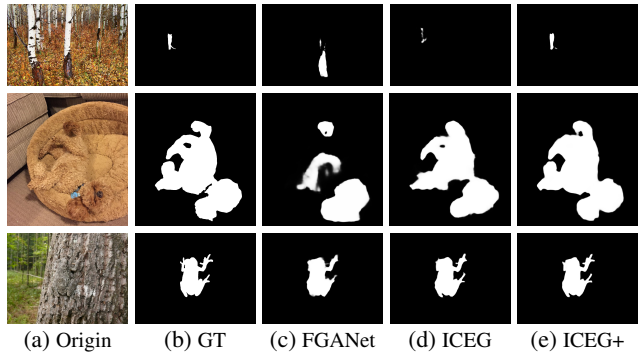


Figure 1: Results of FGANet [40], ICEG, and ICEG+. ICEG+ indicates to optimize ICEG under the *Camouflageator* framework. Both ICEG and ICEG+ generate more complete results with clearer edges. ICEG+ also exhibits better localization capacity.

on the other hand, must develop acute vision systems to decipher camouflage tricks.

Camouflaged object detection (COD) is the task that aims to mimic predators' vision systems and localize foreground objects that have subtle differences from the background. The intrinsic similarity between camouflaged objects and the backgrounds renders COD a more challenging task than traditional object detection [20], and has attracted increasing research attention for its potential applications in medical image analysis [13], species discovery [29], and ecological protection [34].

Traditional COD solutions [11, 26] rely on manually designed detection strategies with hand-crafted extractors, and thus are constrained by the limited feature discriminability. Benefiting from the powerful feature extraction capacity of convolutional neural network [10], a series of deep learning-based methods have been proposed and have achieved remarkable success on the COD task [8, 9, 40]. However, when facing some extreme camouflage scenarios, those methods still struggle to excavate sufficient discriminative cues crucial to *precisely* localize objects of interest. For example, as shown in the top row of Fig. 1, the state-of-the-art COD method, FGANet [40], cannot even roughly

*Corresponding author.

localize the object and thus produce a completely wrong result. Sometimes, even though a rough position can be obtained, FGANet still fails to precisely segment the objects, as shown in the middle and bottom rows of Fig. 1. While FGANet manages to find the rough regions for the objects, the results are either incomplete (middle row: some key parts of the dog are missing) or ambiguous (bottom row: the boundaries of the frog are not segmented out).

This paper aims to address these limitations. We are inspired by the prey-vs-predator game, where preys develop more deceptive camouflage skills to escape predators, which, in turn, pushes the predators to develop more acute vision systems to discern the camouflage tricks. This game leads to ever-strategic preys and ever-acute predators. With this inspiration, we propose to address COD by developing algorithms on both the prey side that generates more deceptive camouflage objects and the predator side that produce complete and precise detection results.

On the prey side, we propose a novel adversarial training framework, Camouflageator, which generates more camouflaged objects that make it even harder for existing detectors to detect and thus enhance the generalizability of the detectors. Specifically, as shown in Fig. 2, Camouflageator comprises an auxiliary generator and a detector, which could be any existing detector. We adopt an alternative two-phase training mechanism to train the generator and the detector. In Phase I, we fix the detector and train the generator to synthesize camouflaged objects aiming to deceive the detector. In Phase II, we fix the generator and train the detector to accurately segment the synthesized camouflaged objects. By iteratively alternating Phases I and II, the generator and detector both evolve, helping to obtain better COD results.

On the predator side, we present a novel COD detector, named Internal Coherence and Edge Guidance (ICEG), which particularly aims to address the issues of incomplete segmentation and ambiguous boundaries of existing COD detectors. For incomplete segmentation, we introduce a camouflaged feature coherence (CFC) module to excavate the internal coherence of camouflaged objects. We first explore the feature correlations using two feature aggregation components, *i.e.*, the intra-layer feature aggregation and the contextual feature aggregation. Then, we propose a camouflaged consistency loss to constrain the internal consistency of camouflaged objects. To eliminate ambiguous boundaries, we propose an edge-guided separated calibration (ESC) module. ESC separates foreground and background features using attentive masks to decrease uncertainty boundaries and remove false predictions. Additionally, ESC leverages edge features to adaptively guide segmentation and reinforce the feature-level edge information to achieve the sharp edge for segmentation results.

Our contributions are summarized as follows:

- We introduce an adversarial training framework, Cam-

ouflageator, for the COD task. Camouflageator introduces an auxiliary generator that generates more camouflage objects that are harder for COD detectors to detect and hence enhances the generalizability of the COD detectors. Camouflageator is flexible and can be integrated with various existing COD detectors.

- We propose a new COD detector, ICEG, to address the issues of incomplete segmentation and ambiguous boundaries that existing detectors face. ICEG introduces a novel CFC module to excavate the internal coherence of camouflaged objects to obtain complete segmentation results, and an ESC module to leverage edge information to get precise boundaries.
- Experiments on four datasets verify that Camouflageator can promote the performance of various existing COD detectors, ICEG significantly outperforms existing COD detectors, and integrating Camouflageator with ICEG reaches even better results.

2. Related work

2.1. Camouflaged object detection

Traditional COD methods rely on hand-crafted operators with limited feature discriminability, thus struggling to handle complex scenarios. Learning-based approaches have recently become mainstream in COD with three main categories: (i) *Multi-stage framework*: SegMaR [14] was the first plug-and-play framework for COD task to integrate segment, magnify, and reiterate under a multi-stage framework. However, SegMaR has limitations in flexibility due to not being end-to-end trainable. (ii) *Multi-scale feature aggregation*: PreyNet [42] proposed a bidirectional bridging interaction module to aggregate cross-layer features with attentive guidance. Similarly, FGANet [40] designed a collaborative local information interaction module and a global information interaction module to aggregate structure context features. (iii) *Joint training strategy*: LSR [23] presented the first multi-task framework for COD to simultaneously localize, segment, and rank camouflaged objects using a joint training strategy. Analogously, BGNet [33] jointly trained the edge detection task with the COD task and guided the segmentation with the detected edge.

We improve existing methods in three aspects: (i) Camouflageator is the first end-to-end trainable plug-and-play framework for COD, thus ensuring flexibility. (ii) ICEG is the first COD detector to alleviate incomplete segmentation by excavating the internal coherence of camouflaged objects. (iii) Unlike existing edge-based detectors [39, 33], ICEG employs edge information to guide segmentation adaptively under the separated attentive framework.

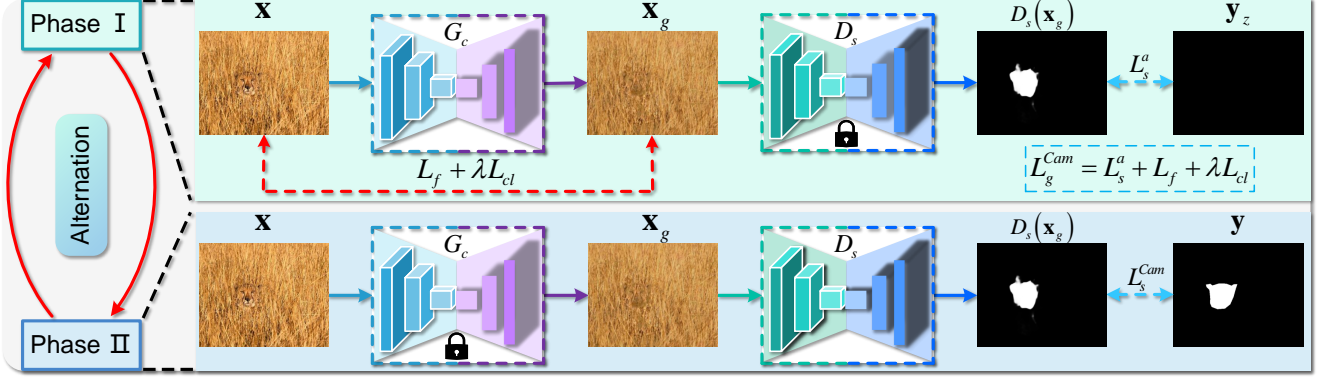


Figure 2: Architecture of Camouflageator. In Phase I, we fix detector D_s and update generator G_c to synthesize more camouflaged objects to deceive D_s . In Phase II, we fix G_c and train the detector D_s to segment the synthesized image.

2.2. Adversarial training

Adversarial training is a widely-used solution with many applications, including adversarial attack [41] and generative adversarial network (GAN) [1, 18]. Recently, several GAN-based methods have been proposed for the COD task. JCOD [17] introduced a GAN-based framework to measure the prediction uncertainty. ADENet [36] employed GAN to weigh the contribution of depth for COD. Distinct from those GAN-based methods, our Camouflageator enhances the generalizability of existing COD detectors by generating more camouflaged objects that are harder to detect.

3. Methodology

When preys develop more deceptive camouflaged skills to escape predators, the predators respond by evolving more acute vision systems to discern the camouflage tricks. Drawing inspiration from this prey-vs-predator game, we propose to address COD by developing the Camouflageator and ICEG algorithms that mimic preys and predators, respectively, to generate more camouflaged objects and to more accurately detect those camouflaged objects.

3.1. Camouflageator

Camouflageator is an adversarial training framework that employs an auxiliary generator G_c to synthesize more camouflaged objects that make it even harder for existing detectors D_s to detect and thus enhance the generalizability of the detectors. We train G_c and D_s alternately in a two-phase adversarial training scheme. Fig. 2 shows the framework.

Training the generator. We fix the detector D_s and train the generator G_c to generate more deceptive objects that fail the detector. Given a camouflaged image \mathbf{x} , we generate

$$\mathbf{x}_g = G_c(\mathbf{x}), \quad (1)$$

and expect \mathbf{x}_g is more deceptive to D_s than \mathbf{x} . To achieve this, \mathbf{x}_g should be visually consistent (similar in global appearance) with \mathbf{x} but have those discriminative features crucial for detection hidden or reduced.

To encourage visual consistency, we propose to optimize the fidelity loss represented by the following formulation:

$$L_f = \|(\mathbf{1} - \mathbf{y}) \otimes \mathbf{x}_g - (\mathbf{1} - \mathbf{y}) \otimes \mathbf{x}\|^2, \quad (2)$$

where \mathbf{y} is the ground truth binary mask and \otimes denotes element-wise multiplication. Since $(\mathbf{1} - \mathbf{y})$ denotes the background mask, this term in essence encourage \mathbf{x}_g to be similar with \mathbf{x} for the background region. We encourage fidelity by preserving only the background rather than the whole image because otherwise, it hinders the generation of camouflaged objects in the foreground.

To hide discriminative features, we optimize the following concealment loss to imitate the bio-camouflage strategies, *i.e.*, internal similarity and edge disruption [30], as

$$L_{cl} = \|\mathbf{y} \otimes \mathbf{x}_g - P_o^I\|^2 + \|\mathbf{y}_e \otimes \mathbf{x}_g - P_e^I\|^2, \quad (3)$$

where \mathbf{y}_e is the weighted edge mask diluted by Gaussian function [14] to capture richer edge information. P_o^I is the image-level object prototype which is an average of foreground pixels. P_e^I is the image-level edge prototype which is an average of edge pixels specified by \mathbf{y}_e . Note that \mathbf{y}_e , P_o^I , and P_e^I are all derived from the provided ground truth \mathbf{y} and help to train the model. This term encourages individual pixels of the foreground region and the edge region of \mathbf{x}_g to be similar to the average values, which has a smooth effect and thus hides discriminative features.

Apart from the above concealment loss, we further employ the detector D_s to reinforce the concealment effect. The idea is that if \mathbf{x}_g is perfectly deceptive, D_s tends to detect nothing as the foreground. To this end, we optimize

$$L_s^a = L_{BCE}^w(D_s(\mathbf{x}_g), \mathbf{y}_z) + L_{IoU}^w(D_s(\mathbf{x}_g), \mathbf{y}_z), \quad (4)$$

where $\mathbf{y}_z = \mathbf{0}$ is an all-zero mask with the same size as \mathbf{y} . $L_{BCE}^w(\cdot)$ and $L_{IoU}^w(\cdot)$ are the weighted binary cross-entropy loss [12] and the weighted intersection-over-union loss [31].

Our overall learning objective to train G_c is as follows,

$$L_g^{Cam} = L_s^a + L_f + \lambda L_{cl}, \quad (5)$$

where λ is the hyper-parameter.

Training the detector. In Phase II, we fix the generator G_c and train the detector D_s to accurately segment the synthe-

layer feature correlations by selectively interacting cross-level information with channel attention and spatial attention [35, 7], which ensures the retention of significant coherence. The aggregated feature $\{f_k^c\}_{k=1}^3$ is:

$$f_k^c = SA(CA(conv3(conca(up(f_{k+1}^c), f_k^a))))), \quad (10)$$

where $up(\cdot)$ is up-sampling operation. $CA(\cdot)$ and $SA(\cdot)$ are channel attention and spatial attention. Note that $f_4^c = f_4^a$. Having acquired $\{f_k^c\}_{k=1}^3$, the integrated features $\{f_k^l\}_{k=1}^3$ conveyed to the decoder are formulated as follows:

$$f_k^l = conv1(concate(f_k^a, f_k^c)). \quad (11)$$

We employ $conv1$ for channel integration and $f_4^l = f_4^a$.

Camouflaged consistency loss. To enforce the internal consistency of the camouflaged object, we propose a camouflaged consistency loss to enable more compact internal features. To achieve this, one intuitive idea is to decrease the variance of the camouflaged internal features. However, such a constraint can lead to feature collapse, *i.e.*, all extracted features are too clustered to be separated, thus diminishing the segmentation capacity. Therefore, apart from the above constraint, we propose an extra requirement to keep the internal and external features as far away as possible. We apply the feature-level consistency loss to the deepest feature f_4^l for its abundant semantic information:

$$L_{cc} = \|\mathbf{y}_d \otimes f_4^l - P_o^f\|^2 - \|\mathbf{y}_d \otimes f_4^l - P_b^f\|^2, \quad (12)$$

where \mathbf{y}_d is the down-sampled ground truth mask. P_o^f and P_b^f denote the feature-level prototypes of the camouflaged object and the background, respectively.

Discussions. Apart from focusing on feature correlations as in existing detectors [14, 42], we design a novel camouflaged consistency loss to enhance the internal consistency of camouflaged objects, facilitating complete segmentation.

3.2.2 Edge-guided segmentation decoder

As depicted in Fig. 3, edge-guided segmentation decoder (ESD) $\{D_k\}_{k=1}^4$ comprises an edge reconstruction (ER) module and an edge-guided separated calibration (ESC) module to generate the edge predictions $\{p_k^e\}_{k=1}^4$ and the segmentation results $\{p_k^s\}_{k=1}^5$, respectively.

Edge reconstruction module. We introduce an ER module to reconstruct the object boundary. Assisted by the edge map p_{k+1}^e and the segmentation feature f_{k+1}^s from the former decoder, the edge feature f_k^e is presented as follows:

$$f_k^e = CRB(conca(f_k^l \otimes p_{k+1}^e + f_k^l, f_{k+1}^s)). \quad (13)$$

where $f_5^s = A_s(f_4)$ and $p_k^e = conv3(f_k^e)$. f_5^e and p_5^e are set as zero for initialization. We repeat p_{k+1}^e as a 64-dimension tensor to ensure channel consistency with f_k^l in Eq. (13).

Edge-guided separated calibration module. Ambiguous boundary, a common problem in COD, manifests as a high degree of uncertainty in the fringes and the unclear edge of the segmented object. We have observed that the high degree of uncertainty is mainly due to the intrinsic similarity

between the camouflaged object and the background. To address this issue, we separate the features from the foreground and the background by introducing the corresponding attentive masks, and design a two-branch network to process the attentive features. This approach helps decrease uncertainty fringes and remove false predictions, including false-positive and false-negative errors. Given the prediction map p_{k+1}^s , the network is defined as follows:

$$f_k^s = conca(f_k^{sf}, f_k^{sb}), p_k^s = conv3(f_k^s), \quad (14)$$

where f_k^{sf} and f_k^{sb} are the foreground attentive feature and the background attentive feature, which are formulated as:

$$f_k^{sf} = RCAB(f_k^l \otimes S(p_{k+1}^s) + f_k^l), \quad (15a)$$

$$f_k^{sb} = RCAB(f_k^l \otimes S(R(p_{k+1}^s)) + f_k^l), \quad (15b)$$

where $S(\cdot)$ and $R(\cdot)$ are Sigmoid and reverse operators, *i.e.*, element-wise subtraction with 1. $RCAB(\cdot)$ is the residual channel attention block [43], which is used to emphasize those informative channels and high-frequency information.

The second phenomenon, unclear edge, is due to the extracted features giving insufficient importance to edge information. In this case, we explicitly incorporate edge features to guide the segmentation process and promote edge prominence. Instead of simply superimposing, we design an adaptive normalization (AN) strategy with edge features to guide the segmentation in a variational manner, which reinforces the feature-level edge information and thus ensures the sharp edge of the segmented object. Given the edge feature f_{k+1}^e , the attentive features can be acquired by:

$$f_k^{sf} = \sigma_k^f \otimes (RCAB(f_k^l \otimes S(p_{k+1}^s) + f_k^l)) + \mu_k^f, \quad (16a)$$

$$f_k^{sb} = \sigma_k^b \otimes (RCAB(f_k^l \otimes S(R(p_{k+1}^s)) + f_k^l)) + \mu_k^b, \quad (16b)$$

where $\{\sigma_k^f, \mu_k^f\}$ and $\{\sigma_k^b, \mu_k^b\}$ are the corresponding variational parameters. In AN, $\{\sigma_k, \mu_k\}$ can be calculated by: $\sigma_k = conv3(CRB(f_{k+1}^e))$, $\mu_k = conv3(CRB(f_{k+1}^e))$. (17)

Discussions. Unlike existing edge-guided methods [33, 39] that focus only on edge guidance, we combine edge guidance with foreground/background splitting using attentive masks. This integration enables us to decrease uncertainty fringes and remove false predictions along edges.

3.2.3 Loss functions of ICEG

Apart from the camouflaged consistency loss, our ICEG is also constraint with the segmentation loss L_s and the edge loss L_e to supervise the segmentation results $\{p_k^s\}_{k=1}^5$ and the reconstructed edge results $\{p_k^e\}_{k=1}^4$. Following [3], the segmentation loss L_s consists of $L_{BCE}^w(\cdot)$ and $L_{IoU}^w(\cdot)$:

$$L_s = \sum_{k=1}^5 \frac{1}{2^{k-1}} (L_{BCE}^w(p_k^s, \mathbf{y}) + L_{IoU}^w(p_k^s, \mathbf{y})). \quad (18)$$

For edge supervision, we employ dice loss $L_{dice}(\cdot)$ [25]

to overcome the extreme imbalance in edge maps:

$$L_e = \sum_{k=1}^4 \frac{1}{2^{k-1}} L_{dice}(p_k^e, y_e). \quad (19)$$

Therefore, the total loss is presented as follows:

$$L_t = L_s + L_e + \beta L_{cc}, \quad (20)$$

where β is the trade-off parameter.

3.2.4 ICEG+

To promote the adoption of the proposed Camouflageator, we provide a use case and utilize ICEG+ to denote the algorithm that integrates our Camouflageator framework with ICEG. The integration is straightforward; we only need to replace the detector supervision from Eq. (6) with Eq. (20). In addition, we pre-train ICEG with L_t (Eq. (20)) to ensure the training stability. See Sec. 4.1 for more details.

4. Experiments

4.1. Experimental setup

Implementation details. Both the Camouflageator framework and ICEG detector are implemented on PyTorch on two RTX3090 GPUs. For Camouflageator, the generator adopts ResUNet as its backbone. As for ICEG, a pre-trained ResNet50 [10] on ImageNet [15] is employed as the default encoder. We also report the COD results with other encoders, including Res2Net50 [6] and Swin Transformer [21]. Following [5], we resize the input image as 352×352 and pre-train ICEG by Adam with momentum terms (0.9, 0.999) for 100 epochs. The batch size is set as 36 and the learning rate is initialized as 0.0001, decreased by 0.1 every 50 epochs. Then we use the same batch size to further optimize ICEG under the Camouflageator framework for 30 epochs and get ICEG+, where the optimizer is Adam with parameters (0.5, 0.99) and the initial learning rate is 0.0001, dividing by 10 every 15 epochs. The hyper-parameters λ and β are set as 0.1.

Datasets. We use four COD datasets for evaluation, including CHAMELEON [32], CAMO [16], COD10K [3], and NC4K [23]. CHAMELEON comprises 76 camouflaged images. CAMO contains 1,250 images with 8 categories. COD10K consists of 5,066 images with 10 super-classes. NC4K is the largest test set with 4,121 images. Following the common setting [5, 3], our training set involves 1,000 images from CAMO and 3,040 images from COD10K, and our test set integrates the rest from the four datasets.

Metrics. Following previous methods [5, 3, 14], we employ four commonly-used metrics, including mean absolute error (M), adaptive F-measure (F_β) [24], mean E-measure (E_ϕ) [4], and structure measure (S_α) [2]. Note that smaller M or larger F_β , E_ϕ , S_α signify better performance.

4.2. Comparison with the state-of-the-arts

Quantitative analysis. We compare our ICEG with 13 state-of-the-art (SOTA) solutions in three different settings. Apart from the common setting (single input scale and single stage), two other settings (multiple input scales and multiple stages) are also included for a comprehensive evaluation, where ICEG follows the corresponding practices of ZoomNet [27] and SegMaR [14]. As shown in Tab. 1, ICEG outperforms the SOTAs by a large margin in all settings and backbones. For instance, in the common setting, ICEG overall surpasses the second-best methods in 3.2%, 6.4%, 8.1% with the backbone of ResNet50 (FGANet [40]), Res2Net50 (BSA-Net [44]), Swin Transformer (DTIT [22]). Moreover, we also present the results of detectors optimized under the Camouflageator framework in the common setting. In Tab. 1, Camouflageator generally improves other detectors by 2.8% (PreyNet) and 2.2% (FGANet) and increases our ICEG by 2.5% (ResNet50), 2.3% (Res2Net50), and 1.4% (Swin Transformer), which verifies that our Camouflageator is a plug-and-play framework. Results of the compared methods are generated by their provided models for fairness.

Qualitative analysis. Fig. 5 shows that ICEG gets more complete prediction results than existing methods, especially for large objects whose intrinsic correlations are more dispersed (the last two rows). This substantiates the effectiveness of the the proposed CFC module that excavates the internal coherence of camouflaged objects for generating more complete prediction maps. Moreover, ICEG gets clearer edges for the predictions than the existing methods, thanks to the proposed ESD module that decreases uncertainty fringes and eliminates unclear edges of the segmented object. Moreover, we can see that ICEG+ obtains even better results than ICEG, further verifying the effectiveness of the proposed Camouflageator framework.

4.3. Ablation study and analysis

We conduct the ablation study and analysis on the two largest datasets, *i.e.*, COD10k and NC4K. The results for the most significant components are shown here; more can be found in the supplement material.

Validity of Camouflageator framework. We conduct validity analyses for Camouflageator, including our objective function in Eq. (5) and the adversarial training manner. As shown in Fig. 6, the generator trained without L_g^c produces the images with severe artifacts, while the one trained with fidelity loss L_f only synthesizes visual-appealing images but fails to hide discriminative features. In contrast, the generator trained with the proposed L_g^c generates high-quality images with more camouflaged objects, ensuring the generalizability of the detector (see Tab. 2a). We also compare our Camouflageator framework with the bi-level optimization (BO) framework [19] to verify the advancement of our

Methods	Backbones	CHAMELEON (76 images)				CAMO (250 images)				COD10K (2,026 images)				NC4K (4,121 images)			
		$M \downarrow$	$F_\beta \uparrow$	$E_\phi \uparrow$	$S_\alpha \uparrow$	$M \downarrow$	$F_\beta \uparrow$	$E_\phi \uparrow$	$S_\alpha \uparrow$	$M \downarrow$	$F_\beta \uparrow$	$E_\phi \uparrow$	$S_\alpha \uparrow$	$M \downarrow$	$F_\beta \uparrow$	$E_\phi \uparrow$	$S_\alpha \uparrow$
Common Setting: Single Input Scale and Single Stage																	
MGL-R [39]	ResNet50	0.031	0.825	0.917	0.891	0.088	0.738	0.812	0.775	0.035	0.680	0.851	0.814	0.053	0.778	0.867	0.833
LSR [23]	ResNet50	0.030	0.835	0.935	0.890	0.080	0.756	0.838	0.787	0.037	0.699	0.880	0.804	0.048	0.802	0.890	0.834
UGTR [37]	ResNet50	0.031	0.805	0.910	0.888	0.086	0.747	0.821	0.784	0.036	0.670	0.852	0.817	0.052	0.778	0.874	0.839
SegMaR-1 [14]	ResNet50	0.028	0.828	0.944	0.892	0.072	0.772	0.861	0.805	0.035	0.699	0.890	0.813	0.052	0.767	0.885	0.835
OSFormer [28]	ResNet50	0.028	0.836	0.939	0.891	0.073	0.767	0.858	0.799	0.034	0.701	0.881	0.811	0.049	0.790	0.891	0.832
PreyNet [42]	ResNet50	0.027	0.844	0.948	0.895	0.077	0.763	0.854	0.790	0.034	0.715	0.894	0.813	0.047	0.798	0.887	0.838
FGANet [40]	ResNet50	0.030	0.838	0.944	0.896	0.070	0.769	0.865	0.800	0.032	0.708	0.894	0.803	0.047	0.800	0.891	0.837
ICEG (Ours)	ResNet50	0.027	0.858	0.950	0.899	0.068	0.789	0.879	0.810	0.030	0.747	0.906	0.826	0.044	0.814	0.908	0.849
PreyNet+ (Ours)	ResNet50	0.027	0.856	0.954	0.901	0.074	0.778	0.869	0.808	0.031	0.744	0.908	0.833	0.044	0.821	0.912	0.859
FGANet+ (Ours)	ResNet50	0.029	0.847	0.948	0.899	0.069	0.781	0.877	0.814	0.030	0.735	0.911	0.823	0.045	0.814	0.905	0.854
ICEG+ (Ours)	ResNet50	0.026	0.863	0.952	0.903	0.066	0.805	0.891	0.829	0.028	0.763	0.920	0.843	0.041	0.835	0.922	0.869
SINet V2 [3]	Res2Net50	0.030	0.816	0.942	0.888	0.070	0.779	0.882	0.822	0.037	0.682	0.887	0.815	0.048	0.792	0.903	0.847
BSA-Net [44]	Res2Net50	0.027	0.851	0.946	0.895	0.079	0.768	0.851	0.796	0.034	0.723	0.891	0.818	0.048	0.805	0.897	0.841
BGNet [33]	Res2Net50	0.029	0.835	0.944	0.895	0.073	0.744	0.870	0.812	0.033	0.714	0.901	0.831	0.044	0.786	0.907	0.851
ICEG (Ours)	Res2Net50	0.025	0.869	0.958	0.908	0.066	0.808	0.903	0.838	0.028	0.752	0.914	0.845	0.042	0.828	0.917	0.867
ICEG+ (Ours)	Res2Net50	0.023	0.873	0.960	0.910	0.064	0.826	0.912	0.845	0.026	0.770	0.925	0.853	0.040	0.844	0.928	0.878
ICON [45]	Swin	0.029	0.848	0.940	0.898	0.058	0.794	0.907	0.840	0.033	0.720	0.888	0.818	0.041	0.817	0.916	0.858
DTIT [22]	Swin	0.028	0.851	0.942	0.900	0.050	0.832	0.916	0.857	0.034	0.723	0.896	0.824	0.041	0.821	0.917	0.863
ICEG (Ours)	Swin	0.023	0.860	0.959	0.905	0.044	0.855	0.926	0.867	0.024	0.782	0.930	0.857	0.034	0.855	0.932	0.879
ICEG+ (Ours)	Swin	0.022	0.867	0.961	0.908	0.042	0.861	0.931	0.871	0.023	0.788	0.934	0.862	0.033	0.861	0.937	0.883
Other Setting: Multiple Input Scales (MIS)																	
ZoomNet [27]	ResNet50	0.024	0.858	0.943	0.902	0.066	0.792	0.877	0.820	0.029	0.740	0.888	0.838	0.043	0.814	0.896	0.853
ICEG (Ours)	ResNet50	0.023	0.864	0.957	0.905	0.063	0.802	0.889	0.833	0.028	0.751	0.913	0.840	0.042	0.827	0.911	0.873
Other Setting: Multiple Stages (MS)																	
SegMaR-4 [14]	ResNet50	0.025	0.855	0.955	0.906	0.071	0.779	0.865	0.815	0.033	0.737	0.896	0.833	0.047	0.793	0.892	0.845
ICEG-4 (Ours)	ResNet50	0.024	0.870	0.961	0.907	0.067	0.802	0.884	0.823	0.028	0.755	0.920	0.843	0.043	0.824	0.915	0.860

Table 1: Quantitative comparisons of ICEG and other 13 SOTAs on four benchmarks. SegMaR-1 and SegMaR-4 are SegMaR at one stage and four stages. “+” indicates optimizing the detector under our Camouflageator framework. Swin denotes Swin Transformer [21]. The best results are marked in **bold**. For ResNet50 backbone in the common setting, the best two results are in **red** and **blue** fonts.

Methods	COD10K (2,026 images)				NC4K (4,121 images)				Methods	COD10K (2,026 images)				NC4K (4,121 images)			
	$M \downarrow$	$F_\beta \uparrow$	$E_\phi \uparrow$	$S_\alpha \uparrow$	$M \downarrow$	$F_\beta \uparrow$	$E_\phi \uparrow$	$S_\alpha \uparrow$		$M \downarrow$	$F_\beta \uparrow$	$E_\phi \uparrow$	$S_\alpha \uparrow$	$M \downarrow$	$F_\beta \uparrow$	$E_\phi \uparrow$	$S_\alpha \uparrow$
w/o L_g^c	0.032	0.721	0.899	0.816	0.046	0.795	0.896	0.842	BO w/o L_{cl}	0.030	0.752	0.910	0.832	0.044	0.820	0.913	0.855
w/ L_f	0.030	0.750	0.907	0.834	0.044	0.817	0.911	0.853	BO w/ L_g^c	0.032	0.722	0.895	0.812	0.046	0.803	0.889	0.841
w/ L_g^c	0.028	0.763	0.920	0.843	0.041	0.835	0.922	0.869	AT w/ L_g^c	0.028	0.763	0.920	0.843	0.041	0.835	0.922	0.869

(a) Effect of the fidelity loss L_f and the concealment loss L_{cl} .

(b) Effect of the adversarial training (AT) strategy.

Table 2: Ablation study of Camouflageator. $L_g^c = L_f + \lambda L_{cl}$. “w/” and “w/o” mean with and without. BO is bi-level optimization.

adversarial manner. BO involves the auxiliary generator and the detector in both the training and testing phases without adversarial training. As the concealment loss L_{cl} may limit the performance in such an end-to-end manner, we also report the results optimized without L_{cl} , namely with only fidelity loss L_f and segmentation loss (Eq. (20)). Tab. 2b demonstrates the effect of our adversarial manner.

Effect of CFC and ESD. The efficacy of CFC modules is verified in Tab. 3a. In Tab. 3a, we examine the impact of the CFC module (in (a)) and investigate the effect of individual components in CFC, including feature aggregation components (in (b), (c), and (d)), and L_{cc} (in (e) and (f)). As shown in Tab. 3a (e), our camouflaged consistency loss L_{cc} generally improves our detector by 3.4%, which its positive effect. Furthermore, we demonstrate the superiority of L_{cc} by incorporating L_{cc} into existing cutting-edge detectors, as detailed in the supplementary materials. Additionally, we

present detailed ablation results for ESD in Tab. 3b, where we highlight the benefits of ESD, ESC, separated calibration, adaptive normalization, and the joint strategy to integrate the ER task into the COD task. Moreover, as observed in Tab. 3b, the combination of edge guidance with foreground/background splitting using attentive masks is shown to further boost detection performance. Such discovery can bring insights for the design of edge guidance modules.

Parameter analysis. ICEG+ is optimized by the Camouflageator framework with multiple losses, which are balanced by two hyper-parameters, *i.e.*, λ in Eq. (5) and β in Eq. (20). To analyze their impact, we vary one of the parameters and fix another, and report the results in Fig. 7. Overall, we find that the different coefficient values in the tested range only slightly influence the final segmentation performance and λ and β achieve the optimal results when they are set to 0.1. So we set λ and β to 0.1 each.

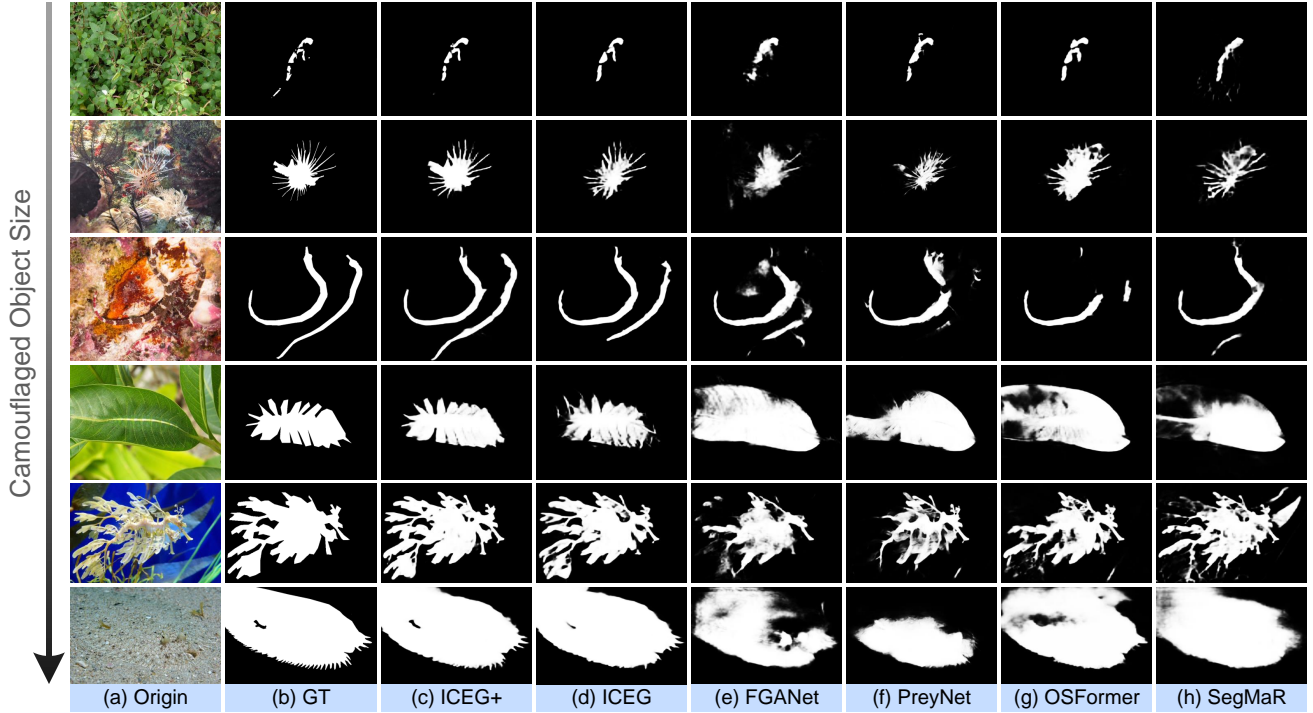


Figure 5: Qualitative analysis of ICEG and other four state-of-the-art techniques, where ICEG generates more complete prediction maps with clearer edges. We also provide the results of ICEG+, which is optimized under the Camouflageator framework.

Methods	COD10K (2,026 images)				NC4K (4,121 images)			
	$M \downarrow$	$F_\beta \uparrow$	$E_\phi \uparrow$	$S_\alpha \uparrow$	$M \downarrow$	$F_\beta \uparrow$	$E_\phi \uparrow$	$S_\alpha \uparrow$
(a) w/o CFC	0.035	0.685	0.866	0.808	0.048	0.781	0.884	0.830
(b) w/o IFA	0.032	0.728	0.885	0.814	0.046	0.782	0.901	0.835
(c) w/o CFA	0.031	0.731	0.893	0.822	0.046	0.803	0.898	0.842
(d) w/o FA	0.033	0.720	0.883	0.812	0.047	0.782	0.893	0.832
(e) w/o L_{cc}	0.032	0.722	0.887	0.816	0.047	0.788	0.889	0.833
(f) $L_{cc}^1 \rightarrow L_{cc}$	0.032	0.704	0.890	0.813	0.046	0.785	0.895	0.836
(g) ICEG	0.030	0.747	0.906	0.826	0.044	0.814	0.908	0.849

(a) Ablation study of CFC module.

Methods	COD10K (2,026 images)				NC4K (4,121 images)			
	$M \downarrow$	$F_\beta \uparrow$	$E_\phi \uparrow$	$S_\alpha \uparrow$	$M \downarrow$	$F_\beta \uparrow$	$E_\phi \uparrow$	$S_\alpha \uparrow$
(a) w/o ESD	0.035	0.678	0.864	0.802	0.049	0.781	0.885	0.832
(b) w/o ESC	0.034	0.688	0.871	0.806	0.048	0.783	0.894	0.835
(c) FC \rightarrow SC	0.032	0.737	0.896	0.820	0.045	0.808	0.899	0.844
(d) BC \rightarrow SC	0.031	0.741	0.902	0.822	0.046	0.811	0.904	0.842
(e) w/o AN	0.033	0.715	0.890	0.815	0.046	0.794	0.896	0.838
(f) w/o ER	0.034	0.693	0.872	0.804	0.048	0.786	0.892	0.834
(g) ICEG	0.030	0.747	0.906	0.826	0.044	0.814	0.908	0.849

(b) Ablation study of ESD component.

Table 3: Ablation study of ICEG on COD10k [3] and NC4K [23]. “ \rightarrow ” is substitution. (a) FA includes both IFA and CFA. L_{cc}^1 is the first term of L_{cc} in Eq. (12). (b) SC, FC, BC are short for separated (Eq. (16)), foreground (Eq. (16a)), background (Eq. (16b)) calibration. Note that “w/o ER” removes edge predictions, thus including “w/o AN”. The best results are marked in bold.

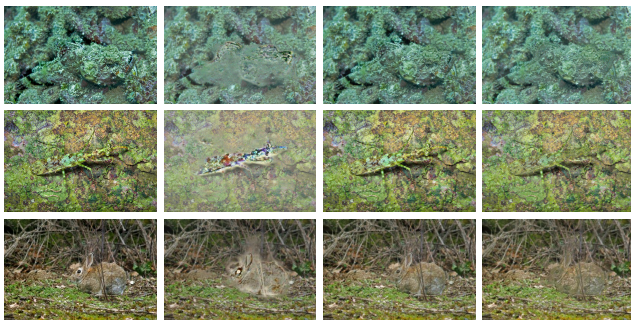


Figure 6: Synthesized images of the generator trained by different losses under the Camouflageator framework. $L_g^c = L_f + \lambda L_{cl}$.

Efficiency analysis. Tab. 4 compares the ResNet50-based SOTAs in terms of parameters and FLOPs, showing that ICEG requires lower computational and memory costs.

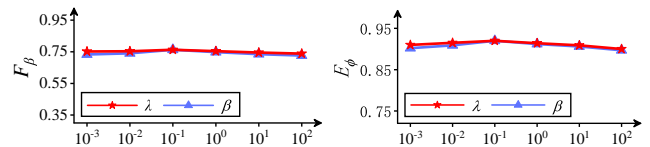


Figure 7: Parameter analysis of λ and β with metrics F_β and E_ϕ .

Costs	SegMaR [14]	OSFormer [28]	PreyNet [42]	FGANet [40]	ICEG
Parameters	55.62	48.74	55.63	51.74	42.76
FLOPs	67.18	52.93	68.63	53.52	48.12

Table 4: Comparisons of Parameters (M) and FLOPs (G) with some cutting-edge methods with the images resized as 352×352 .

5. Conclusion

In this paper, we propose to address COD on both the prey and predator sides. On the prey side, we introduce a novel adversarial training strategy, Camouflageator, to enhance the generalizability of the detector by generating

more camouflaged objects harder for a COD detector to detect. On the predator side, we design a novel detector, dubbed ICEG, to address the issues of incomplete segmentation and ambiguous boundaries. In specific, ICEG employs the CFC module to excavate the internal coherence of camouflaged objects and applies the ESD module for edge prominence, thus producing complete and precise detection results. Extensive experiments demonstrate the effectiveness of Camouflageator and the superiority of ICEG.

References

- [1] Lizhen Deng, Chunming He, Guoxia Xu, Hu Zhu, and Hao Wang. Pcgan: A noise robust conditional generative adversarial network for one shot learning. *IEEE Trans. Intell. Transp. Syst.*, 23(12):25249–25258, 2022. **3**
- [2] Deng-Ping Fan, Ming-Ming Cheng, Yun Liu, Tao Li, and Ali Borji. Structure-measure: A new way to evaluate foreground maps. In *ICCV*, pages 4548–4557, 2017. **6**
- [3] Deng-Ping Fan, Ge-Peng Ji, Ming-Ming Cheng, and Ling Shao. Concealed object detection. *IEEE Trans. Pattern Anal. Mach. Intell.*, 2021. **5, 6, 7, 8**
- [4] Deng-Ping Fan, Ge-Peng Ji, Xuebin Qin, and Ming-Ming Cheng. Cognitive vision inspired object segmentation metric and loss function. *Sci. Sin. Inf.*, 6:6, 2021. **6**
- [5] Deng-Ping Fan, Ge-Peng Ji, Guolei Sun, Ming-Ming Cheng, Jianbing Shen, and Ling Shao. Camouflaged object detection. In *CVPR*, pages 2777–2787, 2020. **6**
- [6] Shang-Hua Gao, Ming-Ming Cheng, Kai Zhao, Xin-Yu Zhang, Ming-Hsuan Yang, and Philip Torr. Res2net: A new multi-scale backbone architecture. *IEEE Trans. Pattern Anal. Mach. Intell.*, 43(2):652–662, 2019. **6**
- [7] Chunming He, Kai Li, Guoxia Xu, Jiangpeng Yan, Longxiang Tang, Yulun Zhang, Xiu Li, and Yaowei Wang. Hqgnet: Unpaired medical image enhancement with high-quality guidance. *arXiv preprint arXiv:2307.07829*, 2023. **5**
- [8] Chunming He, Kai Li, Yachao Zhang, Longxiang Tang, Yulun Zhang, Zhenhua Guo, and Xiu Li. Camouflaged object detection with feature decomposition and edge reconstruction. In *CVPR*, 2023. **1**
- [9] Chunming He, Kai Li, Yachao Zhang, Guoxia Xu, Longxiang Tang, Yulun Zhang, Zhenhua Guo, and Xiu Li. Weakly-supervised concealed object segmentation with sam-based pseudo labeling and multi-scale feature grouping. *arXiv preprint arXiv:2305.11003*, 2023. **1**
- [10] Kaiming He, Xiangyu Zhang, Shaoqing Ren, and Jian Sun. Deep residual learning for image recognition. In *CVPR*, pages 770–778, 2016. **1, 4, 6**
- [11] Jianqin Yin Yanbin Han Wendi Hou and Jinping Li. Detection of the mobile object with camouflage color under dynamic background based on optical flow. *Procedia Eng.*, 15:2201–2205, 2011. **1**
- [12] Shruti Jadon. A survey of loss functions for semantic segmentation. In *CIBCB*, pages 1–7. IEEE, 2020. **3**
- [13] Wei Ji, Shuang Yu, Junde Wu, Kai Ma, Cheng Bian, Qi Bi, Jingjing Li, Hanruo Liu, Li Cheng, and Yefeng Zheng. Learning calibrated medical image segmentation via multi-rater agreement modeling. In *CVPR*, pages 12341–12351, 2021. **1**
- [14] Qi Jia, Shuilian Yao, Yu Liu, Xin Fan, Risheng Liu, and Zhongxuan Luo. Segment, magnify and reiterate: Detecting camouflaged objects the hard way. In *CVPR*, pages 4713–4722, 2022. **2, 3, 5, 6, 7, 8**
- [15] Alex Krizhevsky, Ilya Sutskever, and Geoffrey E Hinton. Imagenet classification with deep convolutional neural networks. *Commun. ACM*, 60(6):84–90, 2017. **6**
- [16] Trung-Nghia Le, Tam V Nguyen, Zhongliang Nie, Minh-Triet Tran, and Akihiro Sugimoto. Anabranh network for camouflaged object segmentation. *Comput. Vis. Image Underst.*, 184:45–56, 2019. **6**
- [17] Aixuan Li, Jing Zhang, Yunqiu Lv, Bowen Liu, Tong Zhang, and Yuchao Dai. Uncertainty-aware joint salient object and camouflaged object detection. In *CVPR*, pages 10071–10081, 2021. **3**
- [18] Kai Li, Yulun Zhang, Kunpeng Li, and Yun Fu. Adversarial feature hallucination networks for few-shot learning. In *Proceedings of the IEEE/CVF conference on computer vision and pattern recognition*, pages 13470–13479, 2020. **3**
- [19] Jinyuan Liu, Xin Fan, Zhanbo Huang, Guanyao Wu, Risheng Liu, Wei Zhong, and Zhongxuan Luo. Target-aware dual adversarial learning and a multi-scenario multi-modality benchmark to fuse infrared and visible for object detection. In *CVPR*, 2022. **6**
- [20] Li Liu, Wanli Ouyang, Xiaogang Wang, Paul Fieguth, Jie Chen, Xinwang Liu, and Matti Pietikäinen. Deep learning for generic object detection: A survey. *Int. J. Comput. Vis.*, 128(2):261–318, 2020. **1**
- [21] Ze Liu, Yutong Lin, Yue Cao, Han Hu, Yixuan Wei, Zheng Zhang, Stephen Lin, and Baining Guo. Swin transformer: Hierarchical vision transformer using shifted windows. In *ICCV*, pages 10012–10022, 2021. **6, 7**
- [22] Zhengyi Liu, Zhili Zhang, Yacheng Tan, and Wei Wu. Boosting camouflaged object detection with dual-task interactive transformer. In *ICPR*, pages 140–146. IEEE, 2022. **6, 7**
- [23] Yunqiu Lv, Jing Zhang, Yuchao Dai, Aixuan Li, Bowen Liu, Nick Barnes, and Deng-Ping Fan. Simultaneously localize, segment and rank the camouflaged objects. In *CVPR*, pages 11591–11601, 2021. **2, 6, 7, 8**
- [24] Ran Margolin, Lihi Zelnik-Manor, and Ayellet Tal. How to evaluate foreground maps? In *CVPR*, pages 248–255, 2014. **6**
- [25] Fausto Milletari, Nassir Navab, and Seyed-Ahmad Ahmadi. V-net: Fully convolutional neural networks for volumetric medical image segmentation. In *3DV*, pages 565–571. IEEE, 2016. **5**
- [26] Yuxin Pan, Yiwang Chen, Qiang Fu, Ping Zhang, and Xin Xu. Study on the camouflaged target detection method based on 3d convexity. *Mod. Appl. Sci.*, 5(4):152, 2011. **1**
- [27] Youwei Pang, Xiaoqi Zhao, Tian-Zhu Xiang, Lihe Zhang, and Huchuan Lu. Zoom in and out: A mixed-scale triplet network for camouflaged object detection. In *CVPR*, pages 2160–2170, 2022. **6, 7**

- [28] Jialun Pei, Tianyang Cheng, Deng-Ping Fan, He Tang, Chuanbo Chen, and Luc Van Gool. Osformer: One-stage camouflaged instance segmentation with transformers. In *ECCV*, pages 19–37. Springer, 2022. 7, 8
- [29] Ricardo Pérez-de la Fuente, Xavier Delclòs, Enrique Peñalver, Mariela Speranza, Jacek Wierzechos, Carmen Ascaso, and Michael S Engel. Early evolution and ecology of camouflage in insects. *Proc. Natl. A. Sci.*, 109(52):21414–21419, 2012. 1
- [30] Natasha Price, Samuel Green, Jolyon Troscianko, Tom Tregenza, and Martin Stevens. Background matching and disruptive coloration as habitat-specific strategies for camouflage. *Sci. Rep.*, 9(1):1–10, 2019. 3
- [31] Md Atiqur Rahman and Yang Wang. Optimizing intersection-over-union in deep neural networks for image segmentation. In *ISVC*, pages 234–244. Springer, 2016. 3
- [32] Przemysław Skurowski, Hassan Abdulameer, J Błaszczuk, Tomasz Depta, Adam Kornacki, and P Koziel. Animal camouflage analysis: Chameleon database. *Unpublished manuscript*, 2(6):7, 2018. 6
- [33] Yujia Sun, Shuo Wang, Chenglizhao Chen, and Tian-Zhu Xiang. Boundary-guided camouflaged object detection. *arXiv preprint arXiv:2207.00794*, 2022. 2, 5, 7
- [34] Evan C Wilson, Amy A Shipley, Benjamin Zuckerberg, M Zachariah Peery, and Jonathan N Pauli. An experimental translocation identifies habitat features that buffer camouflage mismatch in snowshoe hares. *Conserv. Lett.*, 12(2):e12614, 2019. 1
- [35] Sanghyun Woo, Jongchan Park, Joon-Young Lee, and In So Kweon. Cbam: Convolutional block attention module. In *ECCV*, pages 3–19, 2018. 5
- [36] Mochu Xiang, Jing Zhang, Yunqiu Lv, Aixuan Li, Yiran Zhong, and Yuchao Dai. Exploring depth contribution for camouflaged object detection. *arXiv e-prints*, pages arXiv–2106, 2021. 3
- [37] Fan Yang, Qiang Zhai, Xin Li, Rui Huang, Ao Luo, Hong Cheng, and Deng-Ping Fan. Uncertainty-guided transformer reasoning for camouflaged object detection. In *ICCV*, pages 4146–4155, 2021. 7
- [38] Maoke Yang, Kun Yu, Chi Zhang, Zhiwei Li, and Kuiyuan Yang. Denseaspp for semantic segmentation in street scenes. In *CVPR*, pages 3684–3692, 2018. 4
- [39] Qiang Zhai, Xin Li, Fan Yang, Chenglizhao Chen, Hong Cheng, and Deng-Ping Fan. Mutual graph learning for camouflaged object detection. In *CVPR*, pages 12997–13007, 2021. 2, 5, 7
- [40] Wei Zhai, Yang Cao, Jing Zhang, and Zheng-Jun Zha. Exploring figure-ground assignment mechanism in perceptual organization. In *NIPS*, volume 35, 2022. 1, 2, 6, 7, 8
- [41] Chaoning Zhang, Philipp Benz, Chenguo Lin, Adil Karjauv, Jing Wu, and In So Kweon. A survey on universal adversarial attack. *arXiv preprint arXiv:2103.01498*, 2021. 3
- [42] Miao Zhang, Shuang Xu, Yongri Piao, Dongxiang Shi, Shusen Lin, and Huchuan Lu. Preynet: Preying on camouflaged objects. In *ACM MM*, pages 5323–5332, 2022. 2, 5, 7, 8
- [43] Yulun Zhang, Kunpeng Li, Kai Li, Lichen Wang, Bineng Zhong, and Yun Fu. Image super-resolution using very deep residual channel attention networks. In *ECCV*, pages 286–301, 2018. 5
- [44] Hongwei Zhu, Peng Li, Haoran Xie, Xuefeng Yan, Dong Liang, Dapeng Chen, Mingqiang Wei, and Jing Qin. I can find you! boundary-guided separated attention network for camouflaged object detection. In *AAAI*, 2022. 6, 7
- [45] Mingchen Zhuge, Deng-Ping Fan, Nian Liu, Dingwen Zhang, Dong Xu, and Ling Shao. Salient object detection via integrity learning. *IEEE Trans. Pattern Anal. Mach. Intell.*, 2022. 7